

Chiral Voltage Propagation and Calibration in a Topoelectrical Chern Circuit

Tobias Hofmann,^{1,†} Tobias Helbig,^{1,†} Ching Hua Lee,^{2,3} Martin Greiter,¹ and Ronny Thomale^{1,*}

¹*Institute for Theoretical Physics and Astrophysics, University of Würzburg,
D-97074 Würzburg, Germany*

²*Department of Physics, National University of Singapore, Singapore 117542, Singapore*

³*Institute of High Performance Computing, A*STAR, Singapore 138632, Singapore*

 (Received 23 November 2018; published 21 June 2019)

We propose an electric circuit array with topologically protected unidirectional voltage modes at its boundary. Instead of external bias fields or Floquet engineering, we employ negative impedance converters with current inversion (INICs) to accomplish a nonreciprocal, time-reversal symmetry-broken electronic network we call a topoelectrical Chern circuit (TCC). The TCC features an admittance bulk gap fully tunable via the resistors used in the INICs, along with a chiral voltage boundary mode reminiscent of the Berry flux monopole present in the admittance band structure. The active circuit elements in the TCC can be calibrated to compensate for dissipative loss.

DOI: [10.1103/PhysRevLett.122.247702](https://doi.org/10.1103/PhysRevLett.122.247702)

Introduction.—The Chern Insulator (CI) is a cornerstone of topological band theory. It is understood as the lattice version of a quantum Hall system with topologically protected edge modes, which are located in the spectral gap characterizing the bulk insulating state. Conceived by Haldane as a tight-binding model of electrons with broken time-reversal symmetry on a hexagonal lattice [1], it is rooted in the Berry phase experienced by the electrons within the Brillouin zone viewed as a compact parameter space [2,3]. The lattice Chern number C is quantized to take integer values, as it counts the total charge of Berry flux monopoles. For a CI with open boundaries, this implies C chiral edge modes which are topologically protected against disorder and other imperfections, due to the absence of backscattering. This induces a stronger protection than, for instance, topological insulators, where only elastic backscattering is prohibited by the time-reversal symmetry-protected topological character.

As the Berry phase is a phenomenon of parameter space and does not rely on any property of the phase space of quantum electrons, the CI suggests itself for a plethora of alternative realizations. Haldane and Raghu employed this insight to propose a CI in photonic crystals by use of the Faraday effect, where chiral edge modes would manifest as one-way waveguides [4]. This work inspired the formulation and realization of Chern bands in magneto-optical photonic crystals [5,6], optical waveguides subject to a magnetic field [7] or Floquet modulation [8], ultracold atomic gases [9], mechanical gyrotropic [10–12] and acoustic [13,14] systems, as well as, most recently, coupled optical resonators [15] and exciton polariton metamaterials [16]. The nature and potential technological use of topological chiral edge modes crucially depends on the constituent degrees of freedom, the magnitude of the bulk gap,

and the ability to prevent loss from affecting the edge dynamics. In all before-mentioned physical systems, the latter is the most challenging aspect, since the edge signal can exhibit significant decay despite its topological protection.

In this Letter, we propose a Chern circuit which is formed by the admittance band structure of an electric network. As initially accomplished for a doubled Hofstadter model [17,18], topoelectrical circuits [19,20] have been found to host topological admittance band structures [21] of high complexity, including Weyl bands [19,22,23] as well as higher-order topological insulators [24–26]. Moving beyond the realm of RLC circuits, the combined time-reversal symmetry and circuit reciprocity breaking through negative impedance converters with current inversion (INICs) [27] allows us to formulate a topoelectrical Chern circuit (TCC) without external bias fields or Floquet engineering. We find topologically protected chiral voltage edge modes which, from the viewpoint of electrical engineering, bear resemblance to a voltage circulator. In contrast to previous Chern band realizations, our arrangement of active circuit elements allows for a recalibration of gain and loss to protect the chiral voltage signal from decay.

Topoelectrical Chern circuit.—The TCC is formed by a periodic circuit structure sketched in Fig. 1(a). The circuit unit cell detailed in Fig. 1(b) consists of two nodes, each of which is connected to three adjacent nodes through a capacitor C_0 and to six next-nearest neighbors through INICs [28], as specified in Fig. 1(c). The nodes are grounded by inductors L_0 as well as capacitors of capacitance $C_g \pm \Delta$ on alternating sublattices A and B . In light of the graph nature of electric circuits implying a gauge degree of freedom for arranging the circuit components in real space [21], we fix the Bravais vectors as $\mathbf{a}_1 = (1, 0)$ and

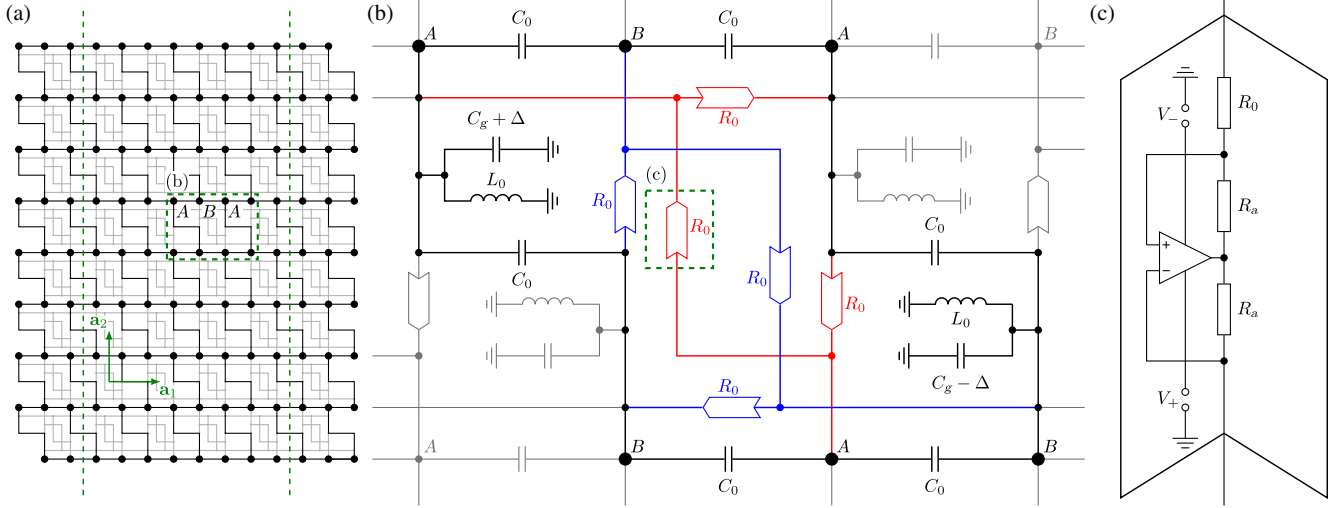


FIG. 1. Topoelectrical Chern circuit. (a) The three-coordinated circuit graph in a brick wall representation of horizontal (x) and vertical (y) alignment of nodes, where the circuit unit cell is given by two “sublattice” nodes A and B , the Bravais vectors by \mathbf{a}_1 and \mathbf{a}_2 , and the x terminations by the vertical green dashed lines. (b) The circuit element structure is detailed for the green dashed framed rectangle in (a). Aside from capacitive internode connections (C_0), there are inductive (L_0) and capacitive ($C_g \pm \Delta$) connections to ground. Further A - A and B - B circuit elements are two oppositely circular sets of INICs (blue and red) labeled by their resistive parameter R_0 . (c) The INIC element structure is shown for the green dashed framed rectangle in (b). The arrangement of resistors R_a and R_0 combined with an operational amplifier with supply voltages V_+ and V_- acts as a negative impedance converter with current inversion, i.e., as a positive (negative) resistor from the front (back) end [28].

$\mathbf{a}_2 = (0, 1)$, amounting to a brick wall structure shown in Fig. 1(a). The brick wall configuration is equivalent to any other arrangement of voltage nodes in real space as long as the connectivity is preserved, and the chosen gauge does not impact any observable quantity [21]. The grounded circuit Laplacian J is defined as the matrix relating the

vector of voltages \mathbf{V} measured with respect to ground to the vector of input currents \mathbf{I} at the N circuit nodes by $\mathbf{I} = J\mathbf{V}$ [19]. For an ac frequency $\omega = 2\pi f$ and two-dimensional reciprocal space implied by the brick wall gauge, the TCC Laplacian $J_{\text{TCC}}(\mathbf{k}; \omega)$ and its spectrum of eigenvalues $j_{\text{TCC}}(\mathbf{k}; \omega)$ reads

$$J_{\text{TCC}}(\mathbf{k}; \omega) = i\omega \left[\left(3C_0 + C_g - \frac{1}{\omega^2 L_0} \right) \mathbb{1} - C_0 [1 + \cos(k_x) + \cos(k_y)] \sigma_x - C_0 [\sin(k_x) + \sin(k_y)] \sigma_y + \left[\Delta + \frac{2}{\omega R_0} [\sin(k_x) - \sin(k_y) - \sin(k_x - k_y)] \right] \sigma_z \right], \quad (1)$$

$$j_{\text{TCC}}(\mathbf{k}; \omega) = i\omega \left[\left(3C_0 + C_g - \frac{1}{\omega^2 L_0} \right) \pm \sqrt{C_0^2 [3 + 2\cos(k_x) + 2\cos(k_x - k_y) + 2\cos(k_y)] + \left(\Delta + \frac{\Gamma(\mathbf{k})}{\omega} \right)^2} \right], \quad (2)$$

where $\Gamma(\mathbf{k}) = (2/R_0)[\sin(k_x) - \sin(k_y) - \sin(k_x - k_y)]$. In Fig. 2(a), we show the projected band structure $j_{\text{TCC};x}(k_y)$ employing open-boundary conditions in the x direction, as specified in Fig. 1(a). It features chiral admittance modes residing in the admittance gap, reminiscent of the chiral energy modes of a CI. Spectral reflection symmetry of $j_{\text{TCC};x}(k_y)$ around zero admittance [Fig. 2(a)] is accomplished for the frequency $\omega_0 = 2\pi f_0 = 1/\sqrt{3C_0 L_0}$.

Chiral edge modes.—The capacitive grounding parameter Δ appears in (1) as an inversion symmetry-breaking term reminiscent of a Semenoff mass [30]. The topological

character of the model roots in the INIC next-nearest neighbor A - A and B - B coupling elements. They break both time-reversal symmetry and circuit reciprocity via the effective implementation of a negative and positive resistance in the forward and reversed direction of the element, respectively [28]. INICs with clockwise orientation [Fig. 1(b)] effectively act as a voltage circulator, where a voltage profile can travel only in one direction [28]. This implements a circular motion of voltage in the bulk of the TCC. The INIC couplings on different sublattices are oriented such that they break chiral symmetry and introduce a Haldane mass

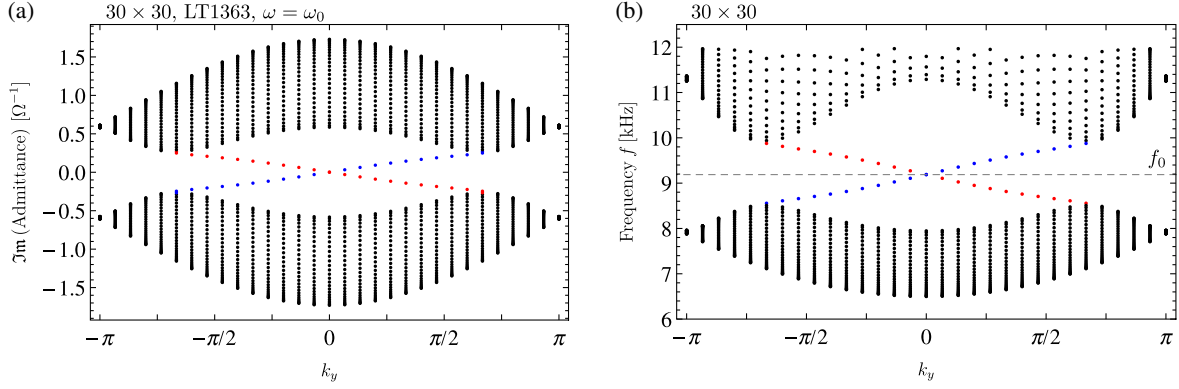


FIG. 2. TCC band structure with a boundary. (a) Admittance band structure $j_{\text{TCC};x}(k_y)$ obtained from LTSPICE simulations for a cylindrical geometry using open boundary conditions with a B - A termination [Fig. 1(a)] in the x direction and periodic boundary conditions in the y direction. The system contains 30 unit cells in the open-boundary direction x and 30 unit cells in the compact direction y . (b) Frequency band structure $\omega(k_y)$ close to the resonance ω_0 obtained from a numerical calculation for the same setting as (a) using the Hamiltonian formalism. TCC parameters are $C_0 = 10 \mu\text{F}$, $L_0 = 10 \mu\text{H}$, $R_0 = 20 \Omega$, $C_g = 0 \text{F}$, $\Delta = 0 \text{F}$, and $f = 9.188 \text{kHz}$. The operational amplifiers are implemented by the LTSPICE model LT1363. A chiral boundary mode for the left (blue) and right (red) x termination is seen in the bulk admittance (a) and the bulk frequency gap (b).

$\Gamma(\mathbf{k})/\omega$. By formal comparison to the Haldane model, (1) amounts to inducing an effective magnetic flux of $\phi = (\pi/2)$ [1]. It is possible to control this fictitious magnetic flux by a modification of the impedance phase of the circuit elements in the INIC [Fig. 1(c)]. The Haldane mass induces a gapped bulk admittance spectrum with chiral edge modes in the admittance gap [Fig. 2(a)].

Symmetries.—The incorporation of resistances in a circuit environment, such as in the TCC, breaks time-reversal symmetry (TRS) [28]. This is because any resistive component experiences Joule heating, leading to increased entropy and, thus, broken time-reversal symmetry. TRS translates into $J = -J^*$ in real space and $J(\mathbf{k}) = -J^*(-\mathbf{k})$ in reciprocal space [28]. We define circuit reciprocity as given by $J^T = J$ in real space and by $J(\mathbf{k}) = J^T(-\mathbf{k})$ in reciprocal space [28]. Using operational amplifiers [31] as active circuit elements, the INIC configuration acts as a charge source or sink, causing an input or output current from ground to the system. Our current feed from the INIC is arranged such that currents between two connected voltage nodes retain equal magnitude but flow in opposite directions. This yields an antisymmetric contribution to J_{TCC} and breaks reciprocity.

We name the TCC Hermitian if J_{TCC} is anti-Hermitian, i.e., $J_{\text{TCC}} = -J_{\text{TCC}}^\dagger$, which leads to imaginary admittance eigenvalues and, hence, real eigenfrequencies $\omega(\mathbf{k})$ [28]. The stationary time evolution of a TCC initial state is then conveniently expressed in terms of TCC energy eigenmodes. J_{TCC} is connected to the TCC's Hamiltonian formulation [28], as the eigenfrequencies $\omega(\mathbf{k})$ are given by the poles of the Greens function $G_{\text{TCC}} = J_{\text{TCC}}^{-1}$ and, hence, relate to the roots of the admittance spectrum $j_{\text{TCC}}(\omega(\mathbf{k})) = 0$ [Fig. 2(b)].

Topological phase diagram.—We define the Chern number for the lower admittance band as $C = (1/2\pi) \oint d^2k \mathcal{B}(\mathbf{k})$,

where $\mathcal{B}(\mathbf{k})$ denotes the Berry curvature [28]. It is invariant under a change of the Bravais vector gauge [21]. As for the Haldane model, from gapping out the two admittance Dirac cones due to a finite Haldane or Semenoff mass, there is a topologically nontrivial (trivial) regime with $C = 1$ ($C = 0$). We find

$$C = \frac{1}{2} \left[\text{sgn} \left(\Delta + \frac{3\sqrt{3}}{\omega R_0} \right) - \text{sgn} \left(\Delta - \frac{3\sqrt{3}}{\omega R_0} \right) \right], \quad (3)$$

which is nonzero if $\omega R_0 < (3\sqrt{3}/\Delta)$. In this case, placing oneself in the admittance or eigenfrequency gap and allowing for a boundary termination, one finds a chiral mode [Figs. 2(a) and 2(b)]. The chiral nature of the voltage boundary mode is rooted in $\omega(\mathbf{k}) \neq \omega(-\mathbf{k})$ associated with the breaking of circuit reciprocity [28] as a necessary condition for $C \neq 0$ in a topoelectrical circuit.

Circuit simulations.—The TCC allows for a detailed characterization and calibration of the chiral voltage boundary mode. Even for a physical system as accessible and tunable as electric circuits, various types of imperfections have to be taken into account. This includes circuit element variances, parasitic resistances, and other constraints on realistic operational amplifiers used in the INICs. The principal timescales and parametric dependencies of the chiral edge mode can be deduced from the clean TCC limit (2), where we set $\Delta = 0$. Within linear approximation of the edge mode in the frequency spectrum [Fig. 2(b)], the group velocities of the zigzag (v_{zz}) and bearded edge (v_{bd}) yield $v_{zz} = (3\sqrt{3}/2\pi)(1/R_0 C_0) = 2v_{bd}$. As seen from (2), the inverse resistance R_0^{-1} serves as a regulation parameter of the gap size. Our numerical analysis indicates that, for sufficiently large values of R_0 (such that $\omega R_0 C_0 \gg 1$),

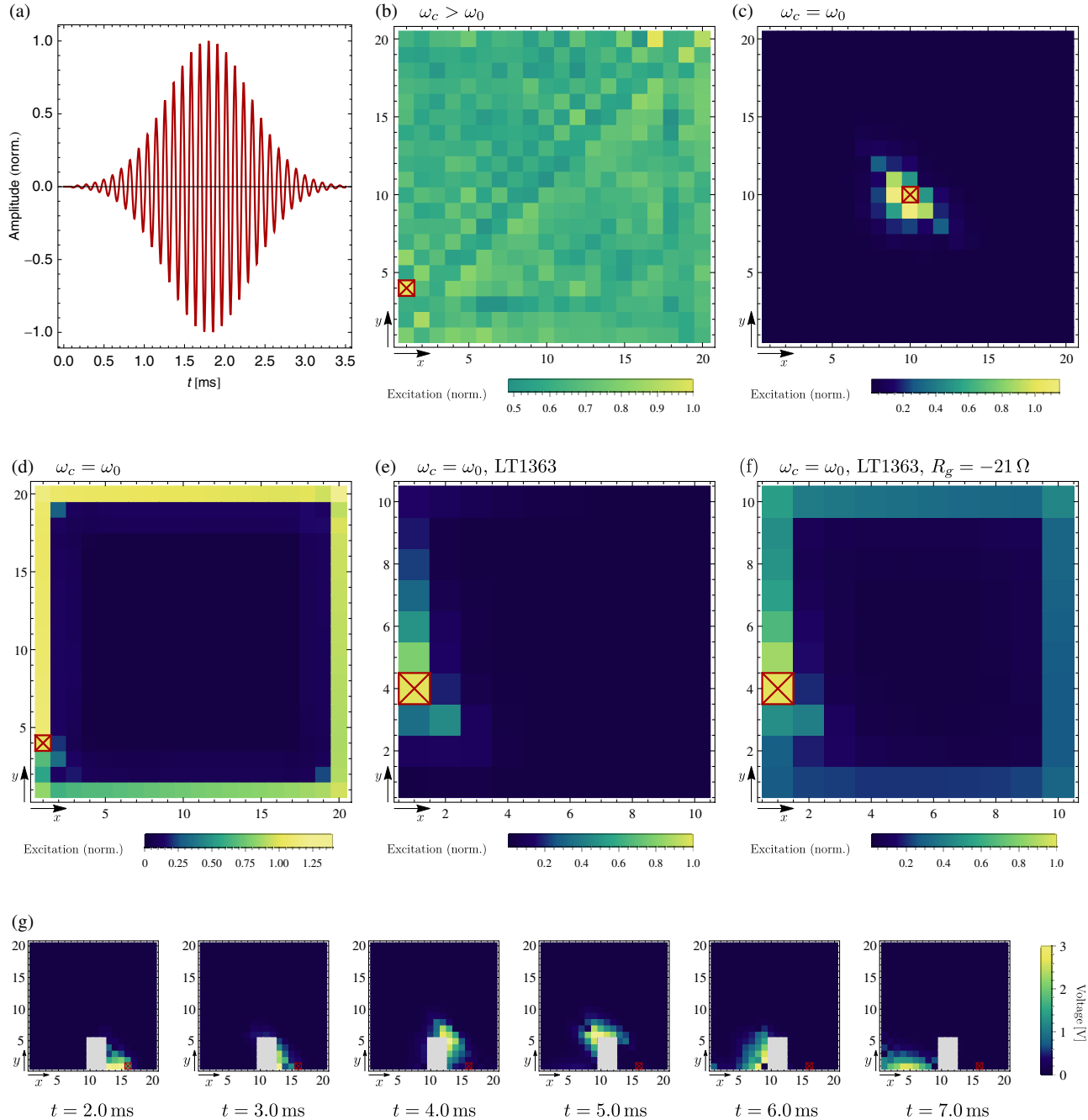


FIG. 3. Simulated current pulse in a finite TCC. (a) An external current signal is fed into the TCC. Its position in (b)–(g) is highlighted by a red crossed square, where all voltage profiles are normalized with respect to the input. (b)–(d) Integrated total voltage signal resolved at each unit cell and obtained from an LTSPICE simulation for (20×20) unit cells with A - B termination with ideal operational amplifiers and parasitic serial resistances of $R_{L_0} = 1 \text{ m}\Omega$ and $R_{C_0} = 0 \text{ m}\Omega$. TCC parameters are $C_0 = 10 \text{ }\mu\text{F}$, $L_0 = 10 \text{ }\mu\text{H}$, $R_0 = 10 \text{ }\Omega$, $\Delta = 0 \text{ F}$, and $C_g = 0 \text{ F}$. (b) $(f_c, \Delta f_{\text{exc}}) = (13.0, 1.0) \text{ kHz}$. The current spreads across the whole circuit. (c) $(f_c, \Delta f_{\text{exc}}) = (9.2, 0.3) \text{ kHz}$. There is a localized circuit response upon bulk injection, as opposed to feeding into the chiral edge mode for a boundary injection (d). (e),(f) $(f_c, \Delta f_{\text{exc}}) = (290, 10) \text{ kHz}$. Integrated total voltage signal for 10×10 unit cells, A - B termination, and realistic operational amplifiers LT1363. $C_0 = 0.1 \text{ }\mu\text{F}$, $L_0 = 1 \text{ }\mu\text{H}$, $R_0 = 30 \text{ }\Omega$, $R_{L_0} = 150 \text{ m}\Omega$, $R_{C_0} = 5 \text{ m}\Omega$, $\Delta = 0 \text{ F}$, and $C_g = 0 \text{ F}$. In comparison to (e), (f) further implements INIC couplings to ground at each edge node, implying an effective negative resistance of $R_g = -21 \text{ }\Omega$ for that connection. The chiral mode signal is significantly enhanced. (g) Time-resolved voltage signal of the TCC with circuit parameters identical to (d) and a defect area of size (3×5) unit cells (gray region) implemented by grounding the corresponding nodes.

the exponential localization of the edge modes is tunable through the resistance R_0 in the INIC [28].

We create a finite TCC lattice, excite it with a Gaussian ac current signal centered around $\omega_c = 2\pi f_c$ and a standard deviation $\Delta\omega_{\text{exc}} = 2\pi\Delta f_{\text{exc}}$, and perform LTSPICE simulations on various configurations (Fig. 3). The time evolution of voltage configurations is modeled by the Hamiltonian formulation of the TCC. If, as in Fig. 3(b), ω_c lies within the TCC frequency band, the current spreads across the whole circuit, even if it is injected at the boundary (marked by a crossed square). If, however, ω_c lies within the bulk gap and $\Delta\omega_{\text{exc}}$ is sufficiently small, the circuit response is crucially different, depending on whether the current is injected in the bulk [Fig. 3(c)] or at the boundary [Fig. 3(d)]. While it is localized for the former, the signal propagates through the chiral edge mode along the boundary for the latter. Note that, due to parasitic effects introduced by the serial resistances of inductors R_{L_0} and capacitors R_{C_0} , the voltage pulse in the circuit faces dissipation caused by the shift of the resonance frequency spectrum along the positive imaginary axis. The most relevant parasitic effects derive from the inductor, introducing a timewise exponential decay constant $\tau = (2L_0/R_{L_0})$ which damps the chiral voltage signal. Our simulation is refined in Figs. 3(e) and 3(f), where we study no idealized, but publicly available operational amplifier elements LT1363. As seen in Fig. 3(e), the realistic setting experiences a significant signal decay already across ten unit cells. In Fig. 3(f), we show one way to calibrate the TCC towards a stable edge signal by adding INIC connections of effective negative resistance R_g between the edge nodes and ground, which effectively yields the insertion of a gain parameter to the system. Through the adjustment of the resistive components in the INICs connected to ground, one can conveniently calibrate the given TCC realization closer towards its Hermitian point, which enhances the Chern mode signal. This is only one of several ways to improve the TCC edge signal through an inherent TCC parameter adjustment. In Fig. 3(f), we implement a defect (gray) area at the boundary of the circuit, in our case by grounding the corresponding voltage nodes. We observe a propagation of the edge mode around the defect, showing the topological protection of the chiral edge mode.

Conclusion.—We have introduced and analyzed the topological Chern circuit as a topological circuit array with active INIC circuit elements. A voltage Chern mode appears due to the nonreciprocity induced by the INICs, which also serve as a calibration tool to minimize the dissipative loss of the Chern mode. This reaches an unprecedented level at which a topological chiral edge mode is tunable in an accessible physical environment and offers itself to further analysis of topological circulator devices.

We thank S. Imhof and A. Stegmaier for helpful discussions. The circuit simulations have been performed

by the use of LTSPICE [32]. The work in Würzburg is supported by the German Research Foundation (DFG) – Project-ID 258499086 – SFB 1170, and by the Würzburg-Dresden Cluster of Excellence on Complexity and Topology in Quantum Matter—*ct.qmat* (EXC 2147, Project-id 39085490).

*Corresponding author.

rthomale@physik.uni-wuerzburg.de

[†]T. Hofmann and T. Helbig equally contributed to this work.

- [1] F. D. M. Haldane, *Phys. Rev. Lett.* **61**, 2015 (1988).
- [2] M. V. Berry, *Proc. R. Soc. A* **392**, 45 (1984).
- [3] J. Zak, *Phys. Rev. Lett.* **62**, 2747 (1989).
- [4] F. D. M. Haldane and S. Raghu, *Phys. Rev. Lett.* **100**, 013904 (2008).
- [5] Z. Wang, Y. D. Chong, J. D. Joannopoulos, and M. Soljačić, *Phys. Rev. Lett.* **100**, 013905 (2008).
- [6] Z. Wang, Y. Chong, J. D. Joannopoulos, and M. Soljačić, *Nature (London)* **461**, 772 (2009).
- [7] Z. Yu, G. Veronis, Z. Wang, and S. Fan, *Phys. Rev. Lett.* **100**, 023902 (2008).
- [8] M. C. Rechtsman, J. M. Zeuner, Y. Plotnik, Y. Lumer, D. Podolsky, F. Dreisow, S. Nolte, M. Segev, and A. Szameit, *Nature (London)* **496**, 196 (2013).
- [9] G. Jotzu, M. Messer, R. Desbuquois, M. Lebrat, T. Uehlinger, D. Greif, and T. Esslinger, *Nature (London)* **515**, 237 (2014).
- [10] C. L. Kane and T. C. Lubensky, *Nat. Phys.* **10**, 39 (2014).
- [11] L. M. Nash, D. Kleckner, A. Read, V. Vitelli, A. M. Turner, and W. T. M. Irvine, *Proc. Natl. Acad. Sci. U.S.A.* **112**, 14495 (2015).
- [12] P. Wang, L. Lu, and K. Bertoldi, *Phys. Rev. Lett.* **115**, 104302 (2015).
- [13] Z. Yang, F. Gao, X. Shi, X. Lin, Z. Gao, Y. Chong, and B. Zhang, *Phys. Rev. Lett.* **114**, 114301 (2015).
- [14] A. B. Khanikaev, R. Fleury, S. H. Mousavi, and A. Alù, *Nat. Commun.* **6**, 8260 (2015).
- [15] M. A. Bandres, S. Wittek, G. Harari, M. Parto, J. Ren, M. Segev, D. N. Christodoulides, and M. Khajavikhan, *Science* **359**, 1231 (2018).
- [16] S. Klemmt, T. H. Harder, O. A. Egorov, K. Winkler, R. Ge, M. A. Bandres, M. Emmerling, L. Worschech, T. C. H. Liew, M. Segev, C. Schneider, and S. Höfling, *Nature (London)* **562**, 552 (2018).
- [17] J. Ningyuan, C. Owens, A. Sommer, D. Schuster, and J. Simon, *Phys. Rev. X* **5**, 021031 (2015).
- [18] V. V. Albert, L. I. Glazman, and L. Jiang, *Phys. Rev. Lett.* **114**, 173902 (2015).
- [19] C. H. Lee, S. Imhof, C. Berger, F. Bayer, J. Brehm, L. W. Molenkamp, T. Kiessling, and R. Thomale, *Commun. Phys.* **1**, 39 (2018).
- [20] L. Lu, *Nat. Phys.* **14**, 875 (2018).
- [21] T. Helbig, T. Hofmann, C. H. Lee, R. Thomale, S. Imhof, L. W. Molenkamp, and T. Kiessling, *Phys. Rev. B* **99**, 161114(R) (2019).
- [22] K. Luo, R. Yu, and H. Weng, *Research* **2018**, 6793752 (2018).

- [23] Y. Lu, N. Jia, L. Su, C. Owens, G. Juzeliūnas, D. I. Schuster, and J. Simon, *Phys. Rev. B* **99**, 020302(R) (2019).
- [24] S. Imhof, C. Berger, F. Bayer, J. Brehm, L. W. Molenkamp, T. Kiessling, F. Schindler, C. H. Lee, M. Greiter, T. Neupert, and R. Thomale, *Nat. Phys.* **14**, 925 (2018).
- [25] M. Serra-Garcia, R. Sūsstrunk, and S. D. Huber, *Phys. Rev. B* **99**, 020304(R) (2019).
- [26] M. Ezawa, *Phys. Rev. B* **98**, 201402(R) (2018).
- [27] W.-K. Chen, *The Circuits and Filters Handbook*, 3rd ed. (CRC Press, Boca Raton, FL, 2009).
- [28] See Supplemental Material at <http://link.aps.org/supplemental/10.1103/PhysRevLett.122.247702> for further information on the negative impedance converter as well as a symmetry and topology classification of the TCC involving the Hamiltonian and the Laplacian formulation, which includes Ref. [29].
- [29] H. Shen, B. Zhen, and L. Fu, *Phys. Rev. Lett.* **120**, 146402 (2018).
- [30] G. W. Semenoff, *Phys. Rev. Lett.* **53**, 2449 (1984).
- [31] Z. Wang, Z. Wang, J. Wang, B. Zhang, J. Huangfu, J. D. Joannopoulos, M. Soljačić, and L. Ran, *Proc. Natl. Acad. Sci. U.S.A.* **109**, 13194 (2012).
- [32] <http://www.linear.com/LTspice>.